Storage, transport, and fate of perfluoroalkyl acids (PFAAs) in a wastewater re-use and groundwater recharge system

Kalle L. Jahn[1]†, Demian M. Saffer[1,2,3], Katherine H. Freeman[1], Sara A. Lincoln[4]

[1] Department of Geosciences, The Pennsylvania State University, University Park, PA, USA

[2] University of Texas Institute for Geophysics, Jackson School of Geosciences, Austin, TX, USA

[3] Department of Geological Sciences, Jackson School of Geosciences, Austin, TX, USA

[4] Energy and Environmental Sustainability Laboratories, The Pennsylvania State University, University Park, PA, USA

Corresponding author: Kalle L. Jahn (kjahn@usgs.gov)

†Current address: USGS New York Water Science Center, Troy, New York, USA

Key points

- Irrigated soils functioned as records of PFAA loading, and estimated historical effluent PFAA loads were much higher than current loads.
- Timing of PFAA leaching differed by four decades depending on PFAA sorption affinity.
- Despite production cessation two decades ago, legacy PFOS stored in vadose zones could remain future source of groundwater contamination.

Abstract

Perfluoroalkyl acids (PFAAs), a group of synthetic compounds associated with adverse human health impacts, are commonly found in effluent discharged from wastewater treatment facilities. When that effluent is used for irrigation, the fate of PFAAs depends strongly on vadose zone solute retention properties and loading history. The relative importance of PFAA retention factors under natural conditions remains uncertain, and the historical record of effluent PFAA concentrations is limited. Using soil cores collected from the Penn State Living Filter (irrigated with treated wastewater effluent for nearly 60 years), we evaluated PFAA transport under near-natural conditions, and estimated historical PFAA concentrations in the irrigated effluent. Total perfluorooctanesulfonic acid (PFOS) and perfluorooctanoic acid (PFOA) masses stored in soils in 2014 were more than 450 times greater than the masses applied during the 2020 effluent irrigation. Equilibrium piston-flow transport models reproduced the observed PFOS and PFOA profiles, allowing us to estimate historical effluent PFOS and PFOA concentrations: 70-170 ng L^{-1} and 1000-1300 ng L^{-1}, respectively. Estimated concentrations were comparable to concentrations measured in other wastewater effluents in the 1990s and 2000s, indicating that when interpreted with transport modeling, wastewater-irrigated soils function as integrated records of historical PFAA loading. Simulated PFOS breakthrough to groundwater occurred 50 years after the start of wastewater irrigation, while simulated PFOA breakthrough occurred after only 10 years of irrigation. Thus, while wastewater irrigation of soils facilitates retention and reduces effluent PFAA loading to surface waters, the resulting increased PFAA storage in soils potentially creates long-term sources of PFAAs to groundwater.

1 Introduction

Perfluoroalkyl acids (PFAAs), a group of synthetic and environmentally persistent compounds associated with adverse human health impacts, have been observed in wastewater treatment plant (WWTP) effluent around the world (Chirikona et al., 2015; Gallen et al., 2018; Houtz et al., 2016; Loganathan et al., 2007; Plumlee et al., 2008; Schultz, Higgins, et al., 2006; Sinclair & Kannan, 2006; W. Zhang et al., 2013). There is also evidence that activated sludge treatment processes promote the transformation of polyfluorinated substances to PFAAs, like perfluorooctanoic acid (PFOA) and perfluorooctanesulfonic acid (PFOS), which are not reactive to treatment processes (Hongrui Chen et al., 2017; Sinclair & Kannan, 2006). Wastewater reuse for agricultural irrigation is an important approach to managing treated wastewater, as it reduces both demand on freshwater sources and the volume of treated wastewater discharged to streams. However, if PFAAs are present in the effluent, they can accumulate in the irrigated soils, which can then become long-term sources of PFAAs to groundwater (Brusseau et al., 2019; Guo et al., 2020; Lyu et al., 2018). PFAA-contaminated groundwater is an important and long-term PFAA exposure vector, as groundwater represents 41% of the American total drinking water supply (public and private) and nearly 99% of private single-household drinking water supply (Dieter et al., 2018). The timing and magnitude of PFAA migration from irrigated wastewater to soils, and subsequently to groundwater, depends primarily on the PFAA retention properties of the irrigated soils and the PFAA effluent loading history.

The unique molecular structure of PFAAs provides them with several phase-behavior mechanisms for retention in soils, including interaction with organic carbon (Higgins & Luthy, 2006), attraction to positively charged mineral surfaces (Hellsing et al., 2016), and accumulation

61 at air-water interfaces (Lyu et al., 2018). Sorption mechanisms are most often studied in
62 laboratory batch and column experiments with concentrated solutions, and there is a dearth of
63 PFAA soil profile data from the field to test the conclusions of these laboratory studies
64 (Brusseau et al., 2020). Additionally, most field studies of PFAA adsorption in vadose zone soils
65 are from sites that received high PFAA loads from aqueous film-forming firefighting foams
66 (Anderson et al., 2019; Bekele et al., 2020; Brusseau et al., 2020; Dauchy et al., 2019). To our
67 knowledge, no field study has investigated PFAA transport and retention in deep soils that have
68 received lower-concentration, decadal-scale irrigation of wastewater effluent.

69 Although waste-water treatment plant (WWTP) discharges account for more than 85% of PFAA
70 releases on continental scales (Sunderland et al., 2019), regular measurements of WWTP
71 effluent PFAA concentrations only began in the mid-2000s (Plumlee et al., 2008; X. Zhang et al.,
72 2017). In industrialized nations, production rates for two common and widely studied PFAAs,
73 Perfluorooctanesulfonic acid (PFOS) and perfluorooctanoic acid (PFOA), increased steadily from
74 the 1970s to peaks in the 1990s before production phase-outs began in 2000 (Paul et al., 2009;
75 Prevedouros et al., 2006). While these production histories have been used to estimate past
76 WWTP discharges (X. Zhang et al., 2017), there are few pre-2000 records of WWTP PFAA
77 concentrations to validate those estimates. This record gap prevents a comprehensive
78 cataloguing of the magnitude and distribution of WWTP-derived PFAA contamination of the
79 terrestrial environment.

80 The lack of field studies on PFAA fate in soils and the gaps in PFAA effluent discharge records
81 leave critical unanswered questions about PFAA transport: (1) What soil properties are the best
82 predictors of PFAA transport under natural field conditions? (2) What are the historical PFAA

loads on soils irrigated with wastewater effluent? And (3) How long will PFAAs leach from those soils to groundwater if irrigation effluent PFAA concentrations are reduced? These questions have significant human health risk implications.

We address these questions using soil cores drilled at a wastewater irrigation spray field as records of both soil PFAA retention behavior and historical PFAA effluent concentrations during >50 years of irrigation. Here, we report correlations between soil properties and PFAA concentrations, and we evaluate PFAA loading and transport history using PFAA mass balances and transport models constrained by site operational history, PFAA production history, and adsorption behavior reported in the literature. In addition to contributing a new record of PFAA retention in deep soils under near-natural conditions, our study illustrates how soil PFAA profiles can be used with simple transport models to estimate historical loading. Model results imply higher PFAA loads in the past and constrain the likely range of historical PFAA concentrations. Our results also suggest that, despite the phase-out of PFOS production in the early 2000s, there is a continued risk of long-term leaching of PFOS from wastewater-irrigated soils due to the highly adsorptive nature of PFOS. Meanwhile, less-adsorptive PFAAs like PFOA have likely already undergone significant leaching to groundwater.

2 Materials and

This study was conducted at a wastewater reuse site, “The Living Filter,” where treated wastewater is used for irrigation and artificial groundwater recharge. The study focuses on a sub-region of the site, known as “The Astronomy Site,” which has been irrigated continuously since 1964. Effluent from the Penn State University Park Wastewater Treatment Plant is applied at an average annual rate of ~160 cm yr^{-1} (Walker & Lin, 2008) and precipitation averages ~100

cm yr^{-1} (NOAA averages 1981-2010). Irrigation occurs year-round and is typically applied for 12-hours, followed by 6.5-day rest period.

The Living Filter is characterized by three different land covers: forest, grasses, and crops. Site soils are predominantly Hagerstown silty clay loam and Hublersburg silt loam, with depths to the underlying limestone and dolomite bedrock as great as 30 m below ground surface (bgs) (Parizek et al., 1967). Soil pH in the top 1 m ranges from 5 to 7, and average saturated hydraulic conductivity in the top 1 m is approximately 2 cm hr^{-1} (Andrews et al., 2016). Based on depth to groundwater measurements from 2017, 2018, and 2020, depth to groundwater beneath the Astronomy area typically ranges from 20 to 70 m bgs (Ayers et al., 2017; Penn State Office of the Physical Plant, personal communication).

The site is underlain by the Cambrian Gatesburg Formation, which locally consists of the Mines Member (coarse-grained dolomite with abundant oolitic chert and thin sandy beds at its base) which overlies the Upper Sandy Member (dolomite with interbedded orthoquartzite and sandy dolomite) (Butts & Moore, 1936; Lattman & Parizek, 1964; Siddiqui & Parizek, 1971; Smith, 1969; Wood, 1980). The quartz-rich beds in the Gatesburg can have substantial primary porosity (as great as 20%), while the dolomite-rich beds tend to have porosity <5% (Smith, 1969).

PFAA concentrations were measured by others in site effluent and groundwater between October 2019 and February 2021 (Mroczko et al., 2022). Four of the groundwater wells sampled were located near the soil core locations at the Astronomy Site (Figure *1*), so PFAA concentrations in those wells were used as a constraint on our models.

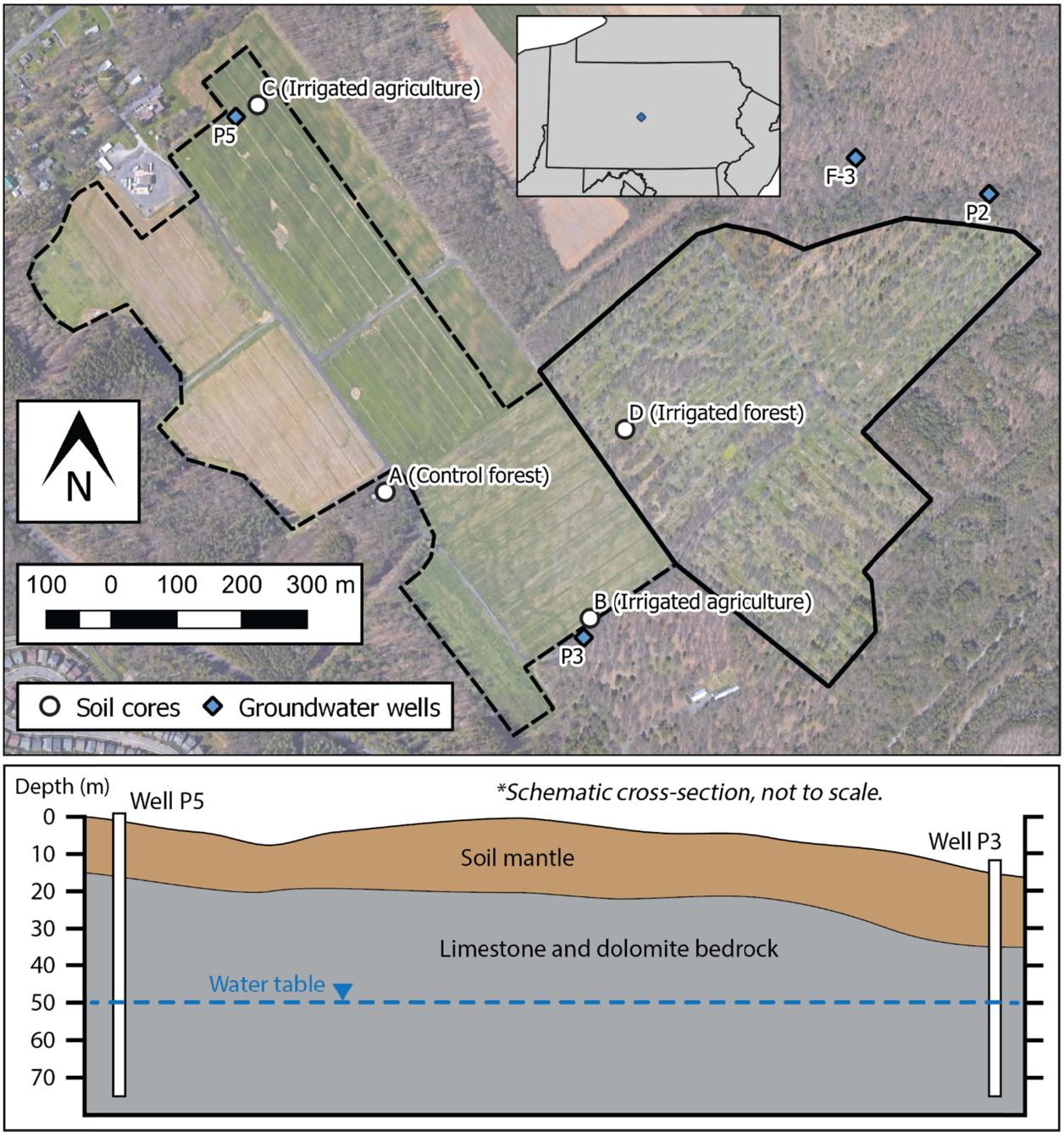

126

127 Figure 1. Satellite image of the Living Filter Astronomy Area in State College, Pennsylvania.
128 White circles denote the locations of cores drilled in 2014, blue diamonds denote groundwater
129 wells sampled for PFAAs in 2020, and black lines denote the area irrigated with treated effluent
130 (solid for forest and dashed for agricultural land). Total irrigated area is approximately 652,000
131 m^2. The schematic cross section below the site map illustrates the approximate range of depths
132 to bedrock and groundwater between wells P5 and P3.

3 Methods

3.1 Soil sampling and characterization

Cores were collected as a part of a Master's thesis (Hagedorn, 2016) investigating the fate of nitrate in the Living Filter. The four core locations included: A) a non-irrigated forest site, B) an irrigated cropland topographic depression, C) an irrigated cropland topographic high, and D) an irrigated forest topographic high (Figure 1). At each location, 7.5-cm diameter soil cores were drilled by hydraulic compression in December 2014 and then sampled at ~30 cm intervals. Samples were analyzed for soil bulk density, particle size distributions, mineralogy, and gravimetric water content at the time of drilling. Following the 2014 sampling, the cores were stored at 4°C in a walk-in refrigeration unit at The Pennsylvania State University. In 2019, 42 of the original sample depths were analyzed for PFAAs, total organic carbon, and bulk elemental composition.

Dry bulk density was measured by inserting a cylindrical metal tube of known volume into the soil core at the selected depths and weighing that sample following oven drying at 105°C for 24 hours. Particle size distributions from 0.06 µm to 880 µm were measured by laser diffraction (Malvern Mastersizer 3000) at the Pennsylvania State University Materials Characterization Lab. Distributions were segregated by Wentworth size classes (clay: <3.9 µm, silt: 3.9-63 µm, sand: 63-880 µm) to characterize soil textures. Gravimetric soil water content was calculated by dividing the change in soil sample mass after oven drying (105°C for 24 hours) by the soil dry mass.

Iron and aluminum content, intended to function as proxies for relative differences of clay and iron oxide content in the cores, were measured with a handheld x-ray fluorescence (XRF)

analyzer (Delta DPO-2000) set to the “Mining Plus” setting and calibrated to a manufacturer-supplied standard. Additionally, 12 samples (samples taken from the top, middle, and bottom of each core) were analyzed for silicate mineralogy by X-ray diffraction (XRD) (Malvern Panalytical Empyrean II). Silicate minerals and their relative abundances were identified from peak angles and intensities using the Rietveld method and the International Centre for Diffraction Data and Inorganic Crystal Structure Database.

42 soil samples were analyzed for total carbon (TC) and total organic carbon (TOC) following U.S. Environmental Protection Agency Method 440 (Zimmermann et al., 1997), which is based on carbon mass loss following organic matter combustion. Each soil sample was powdered (<2 mm particle diameter) using a mortar and pestle cleaned with methanol and dichloromethane between samples. Each well-mixed powdered sample was sub-sampled into two aliquots, and one aliquot was heated to 550°C in a muffle furnace for 6 hours to combust all organic carbon. Combusted and non-combusted aliquots were then analyzed for TC (wt%) by elemental analyzer (Elementar Vario Max CN) at the Pennsylvania State University Agricultural Analytical Services Laboratory. TOC (wt%) was calculated as the difference between the pre- and post-combustion aliquots (TOC = pre-combustion TC – post-combustion TC). 9 aliquots (3 pre-combustion and 6 post-combustion) were analyzed twice, and the mean TC from the replicates was used to calculate TOC. Standard errors for final TOC values were calculated as the square root of the sum of squared TC standard errors, all of which were less than 5% of the corresponding TOC values. This analytical method may slightly overestimate TOC, as some carbonate minerals can decompose at temperatures below 550°C, though $CaCO_3$ does not (Zimmermann et al., 1997).

Soil samples were analyzed for 32 per- and polyfluoroalkyls (PFASs) by modified EPA method 537 Rev 1.1 (Table S1) by Eurofins Lancaster Laboratories (Lancaster, PA). Dry-weight PFAS concentrations were calculated based on soil gravimetric water content at the time of analysis. Matrix spikes were performed to test for matrix suppression of the PFAS signals and labeled isotope recoveries were measured to correct results. PFAS method detection limits (MDL) and limits of quantitation (LOQ) are reported in Table S1. For data analysis, detections between the MDL and LOQ were used quantitatively, and non-detections were treated as equivalent to ½ the MDL (Anderson et al., 2019).

3.2 PFAA analyses and profiles

Total PFAA masses stored in the soils below the Living Filter Astronomy spray field were estimated by combining the PFAA results from profiles B, C, and D into an aggregate profile (core A was excluded because it was located outside of the spray field). This representative column was divided into 11 depth intervals (0.0-0.1 m, 0.1-0.25 m, 0.25-0.5 m, 0.5-1 m, 1-2 m, 2-3 m, 3-4 m, 4-5 m, 5-6 m, 6-7 m, and 7-8 m). Within each interval, mean PFAA concentrations (ng kg^{-1}) were multiplied by the mean soil bulk density (kg m^{-3}), the interval thickness (m), and the column unit area (1 m^2). The resulting PFAA masses (ng) were summed to obtain total PFAA mass for the soil column (mass per m^2 land surface area). Dividing these total PFAA masses by 50 years yielded mean annual rates of PFAA accumulation (mass per m^2 land surface area per year) between the start of effluent application in 1964 and the collection of the cores in 2014

3.3 PFOS and PFOA transport modeling

1-D transport models were developed to gain insight into both historical effluent concentrations and viable field-scale K_{oc} values for soils at the site. The models incorporated

199 both spatial and temporal constraints on the Living Filter system, including the 2014 PFAA soil
200 profiles, 2019-2020 groundwater PFAA concentrations, the Living Filter operational timeline
201 and irrigation rates, and previously compiled global PFAA production and emission trends.
202 Transport modeling was limited to PFOS and PFOA because they are historically the most
203 abundant PFAAs and their production history is better documented than other PFAAs (Paul et
204 al., 2009; Prevedouros et al., 2006).

205 The model domain depth was set to 50 m, close to the 2016-2018 mean groundwater depth
206 under the soil core locations (Ayers et al., 2017; Penn State Office of the Physical Plant,
207 personal communication), as well as groundwater depths in 1963 (Parizek et al., 1967). A
208 column of unit area (1 m^2) was divided into 603 elements with equal pore volume (~0.03 m^3)
209 (but varying soil mass) defined by using exponential fits to porosity and bulk density profiles
210 from all four cores (Figure S1a and b). For each element, a soil-water adsorption coefficient (K_d)

211 $$K_d = \frac{\text{ng PFAA/kg soil}}{\text{ng PFAA/L water}} \quad (1)$$

212 was calculated using organic carbon fractions (f_{oc}) derived from an empirical fit to TOC data
213 (Figure S1c) and K_{oc} values within the range reported in the literature (Table S2)

214 $$K_d = K_{oc} \times f_{oc} \quad (2)$$

215 Water and PFOA/PFOS were applied in a stepwise fashion to the top element of the model, and
216 then moved from element to element via piston flow. Each applied water volume was equal to
217 the element pore volumes (~0.03 m^3), corresponding to ~3 cm of recharge. This volume was

equivalent to the mean weekly effluent irrigation rate (3 cm $week^{-1}$), such that each application represented approximately one week of time.

As water and PFOA/PFOS moved through each element, PFOA/PFOS was partitioned between water and the soil of the element as determined by the distribution coefficient K_d. The assumption that concentrations reach equilibrium over the timescale of downward drainage is supported by previous soil and sediment adsorption experiments, which show that as much as ~90% of PFOS and PFOA sorption occurs in less than 10 hours and full adsorption is reached in less than 48 hours (Higgins & Luthy, 2006; Li et al., 2019). The model does not include the production of PFOA/PFOS from the degradation of precursors in the soil column, an assumption that is supported by previous evidence that treatment processes result in substantial transformation of larger precursor compounds to nondegradable PFAAs (Hongrui Chen et al., 2017; Sinclair & Kannan, 2006).

PFAA effluent concentrations are unknown for most of the Living Filter operational history, as PFAA concentrations in Living Filter irrigation effluent were first measured in late 2019. While there are no continuous records of treatment plant effluent PFAA concentrations that cover the early 2000s reduction in PFOS and PFOA production, a reduction trend has been recorded a decade later: between 2009 and 2014, mean concentrations of PFOS and PFOA in municipal WWTP effluent discharging into San Francisco Bay decreased by 47% and 34%, respectively (Houtz et al., 2016). Therefore, the PFOS and PFOA production changes in the 2000s likely resulted in commensurate changes in PFOS and PFOA concentrations in wastewater effluent. This same assumption has been made by others developing global emission inventories of PFOS and PFOA (Paul et al., 2009; Prevedouros et al., 2006; X. Zhang et al., 2017), and is also

reflected in reductions in PFOS and PFOA in human serum around the world (Sunderland et al., 2019).

Based on these previous estimates and observations of PFOS and PFOA historical releases, the post-phase-out change in effluent PFOS and PFOA concentrations at the Living Filter were assumed to occur as a linear decrease between 2000 and 2014 from unknown historical mean concentrations to the effluent concentrations observed in 2020. Although it is a simplification, the 2000-2014 linear reduction in PFOS is supported by the 2012 restriction of PFOS-containing aqueous firefighting foams and the typical 10-year use cycle of PFOS-treated carpets, both of which are significant contributors to PFOS emissions (Paul et al., 2009). The same linear decrease in PFOA is supported by a ~60% reduction in the PFOA parent chemical production between 1999 and 2004 (Prevedouros et al., 2006), and the 2006 PFOA Stewardship Program enacted by the United States Environmental Protection Agency to end PFOA use by 2015 (Sunderland et al., 2019).

To investigate the PFOS and PFOA loading and adsorption conditions that could produce the 2014 profiles, model parameter sweeps were performed to identify best-fitting combinations of K_{oc} and pre-2000 effluent concentrations. The range of K_{oc} was constrained to the range of previously reported K_{oc} values (PFOS: $10^{2.4}$ to $10^{3.8}$ L kg^{-1}, PFOA: $10^{1.9}$ to $10^{2.7}$ L kg^{-1}, see Table S2 for referenced studies). Models were evaluated in a two-step process. First, the fit between the simulated 2014 profiles and the observed 2014 profiles was estimated using the root mean square error (RMSE):

$$\mathrm{RMSE} = \sqrt{\frac{1}{N}\sum_{i=1}^{N}(O_i - S_i)^2} \quad (3)$$

where O_i and S_i represent observed and simulated concentrations, respectively. Second, time series of solution concentrations at 30 and 50-m bgs from the low-RMSE models were compared to the mean 2019-2020 PFOS and PFOA groundwater concentrations. The 50-m depth time series was selected based on the mean groundwater depths, and the 30-m depth was used to assess the sensitivity of the time series results to the choice of depth at which soil drainage reaches the water table.

4 Results

4.1 Soil properties

Variation in bulk density with depth is similar across all four drilling sites, increasing from just over 1.4 g cm^{-3} near the surface to about 1.7 g cm^{-3} at 10.5 m bgs (Figure 2a, Table S3). TOC variation is also similar across all sites, decreasing exponentially with depth from 1-3% in surficial soils to about 0.1% below 1 m bgs (Figure 2b, Table S3 and S4). The exponential decrease in TOC is consistent with previous TOC trends observed at the Living Filter down to 1.2 m bgs (Andrews et al., 2016). Clay size fractions are less uniform with depth across the four cores, ranging from 6 to 21%, although mean clay fractions are about the same in all cores (A: 12.4%, B: 10.8%, C: 14.1%, D: 11.6%). Iron and aluminum contents generally co-vary, and show a general increasing trend over the top 2-4 m bgs. Based on relative mineral abundances in the XRD data, kaolinite is the dominant clay species across all depths at all four sites (Hagedorn, 2016).

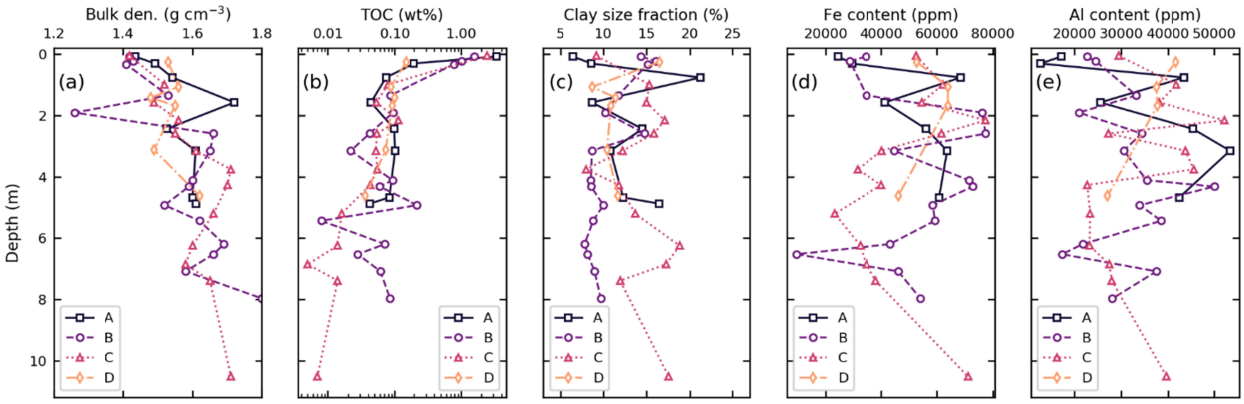

Figure 2. Depth profiles from the four cores for (a) dry bulk density (g cm^{-3}), (b) total organic carbon (wt%), clay particle size fraction (volume, %), (d) iron content (ppm by weight), and aluminum content (ppm by weight)

4.2 PFAA soil profiles and total masses

Only perfluoroalkyl acids (PFAAs) were detected in the soil samples; polyfluoroalkyl compounds were not detected (Table S5). This corroborates past observations that wastewater treatment processes (particularly activated sludge) enhance polyfluoroalkyl substance transformation to PFAAs (Hongrui Chen et al., 2017; Schultz, Higgins, et al., 2006; Sinclair & Kannan, 2006). PFAAs with chain lengths > C10 were only detected once or twice, mostly in a single near-surface sample (5 cm bgs in core C). The majority of PFAAs detections were limited to six structures with carbon chain lengths between C3 and C8 (PFBA, PFPeA, PFHxA, PFOA, PFOS, and PFNA, see Table S1 for full names), so subsequent data analysis focuses on these six PFAAs. When PFAA depth distributions are aggregated into single profiles, some depth distribution patterns emerge (Figure 3 and Figure S2). Most PFPeA, PFOA, PFOS, and PFNA detections are confined to the top 2 m of the profiles, with an apparent exponential decrease with depth. PFBA and PFHxA distributions also decrease with depth, but with more detections down to 6-8 m bgs than the longer-chain PFAAs. The PFBA depth distribution in core A, which was an exception to the

general decreasing-with-depth pattern, exhibited a steady increase from the surface down to 2-3 m bgs.

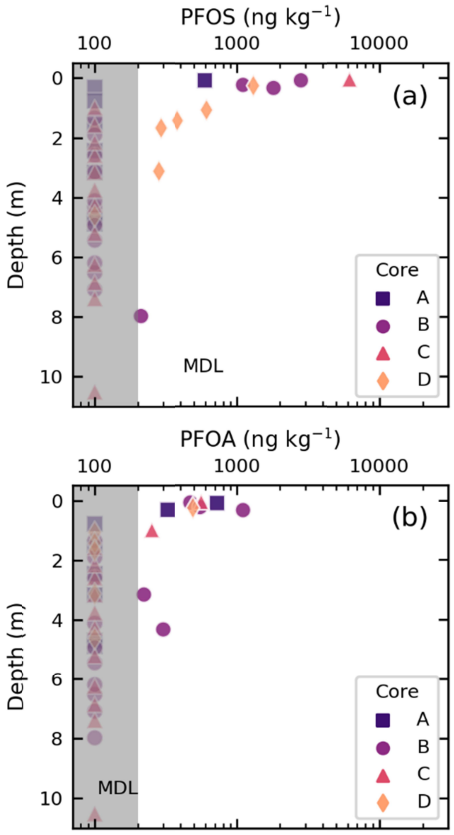

Figure 3. Soil concentration-depth profiles for (a) PFOS and (b) PFOA. Samples are color- and shape-coded by drill site. The sample concentrations that fall below the method detection limit (gray shaded area; MDL < ~200 ng kg^{-1}) are plotted as ½ the method detection limit (MDL) (100 ng kg^{-1}).

Correlations between PFAA concentrations and soil properties were evaluated using Spearman's and Pearson's correlation coefficients (Table 1). Concentrations of PFAAs with carbon chain length 5 or greater all had significant monotonic and linear positive correlations with TOC ($p < 0.05$), with correlation coefficients generally increasing with chain length (Table 1). The lower correlation coefficients between TOC for the shorter-chain PFAAs are consistent with shorter chains having weaker hydrophobic interaction than longer carbon chains. The

amount of the shortest chain PFAA (PFBA) was uncorrelated with TOC, but was monotonically correlated with aluminum and gravimetric water content based on Spearman's coefficient. This is consistent with a greater importance of electrostatic interactions in the sorption of shorter chain PFAAs as previously reported (Zhao et al., 2012). Correlation results indicate TOC was the primary PFAA adsorption control in the Living Filter soils, consistent with the conclusions from previous studies under both field (Anderson et al., 2019) and laboratory conditions (Higgins & Luthy, 2006; Li et al., 2019; Milinovic et al., 2015).

Table 1. Spearman's and Pearson's correlation coefficients and p-values for six PFAAs and five soil property metrics. Statistically significant ($p < 0.05$) correlation coefficients are underlined and bolded.

	PFBA		**PFPeA**		**PFHxA**		**PFOA**		**PFOS**		**PFNA**	
Spearman's	**rho**	**p**	**rho**	**p**	**rho**	**p**	**rho**	**p**	**rho**	**p**	**rho**	**p**
TOC	0.11	0.49	**0.48**	0.00	**0.37**	0.02	**0.53**	0.00	**0.62**	0.00	**0.37**	0.01
GWC	**0.36**	0.02	-0.25	0.11	0.10	0.51	-0.13	0.41	0.00	1.00	0.05	0.76
Clay size	0.14	0.38	0.15	0.36	0.02	0.88	-0.06	0.73	-0.02	0.92	0.02	0.90
Al	**0.37**	0.02	-0.22	0.18	-0.08	0.63	-0.19	0.27	-0.16	0.34	-0.29	0.08
Fe	0.26	0.11	-0.24	0.15	-0.15	0.36	-0.25	0.14	-0.13	0.43	-0.25	0.14
Pearson's	**r**	**p**	**r**	**p**	**r**	**p**	**r**	**p**	**r**	**p**	**r**	**p**
TOC	-0.16	0.31	**0.40**	0.01	**0.38**	0.01	**0.70**	0.00	**0.67**	0.00	**0.44**	0.00
GWC	0.12	0.44	-0.18	0.25	0.05	0.77	-0.08	0.61	-0.04	0.82	0.09	0.55
Clay size	0.07	0.67	0.14	0.36	0.06	0.68	0.02	0.91	-0.03	0.85	0.10	0.55
Al	0.29	0.07	-0.21	0.21	-0.04	0.83	-0.26	0.12	-0.13	0.44	-0.20	0.22
Fe	0.15	0.36	-0.19	0.26	-0.13	0.45	-0.27	0.10	-0.07	0.69	-0.12	0.46

To evaluate the PFAA masses retained in the Living Filter, total PFAA soil profile masses per m^2 land surface area were calculated from aggregated soil profiles (combining cores B, C, and D) for the four PFAAs with 8 or more detections: PFBA (25445 μg m^{-2} land surface area), PFHxA (2438 μg m^{-2}), PFOA (1510 μg m^{-2}), and PFOS (2834 μg m^{-2}). Assuming consistent irrigation from

1964 through 2014 (50 years), the total masses in the column translate to time-averaged annual soil retention of 509 µg PFBA m^{-2} yr^{-1}, 49 µg PFHxA m^{-2} yr^{-1}, 30 µg PFOA m^{-2} yr^{-1}, and 57 µg PFOS m^{-2} yr^{-1}. With the exception of PFHxA, these values are 2-4 orders of magnitude higher than estimated total PFAA masses applied in 2020 (assuming an irrigation rate of 160 cm yr^{-1}): 9 µg PFBA m^{-2} yr^{-1}, 42 µg PFHxA m^{-2} yr^{-1}, 11 µg PFOA m^{-2} yr^{-1}, and 6 µg PFOS m^{-2} yr^{-1}. This requires that prior to 2014, average effluent PFAA concentrations must have been far higher than measured in 2020.

The annually retained masses derived from the mass balance serve as a lower bound on the historical effluent masses: unless dissolved PFAAs were to partition completely to the soil, effluent PFAA masses would have to be higher than the annually retained masses. To provide a conservative estimate of the historical PFAA concentrations needed to produce the observed soil PFOS and PFOA concentrations, we reconstructed equilibrium water concentrations using the soil data. To accomplish this, Equation 2 was used to calculate a K_d value for each soil sample using the relevant sample f_{oc} and the mean K_{oc} value reported in the literature (Table S2). Then, Equation 1 was rearranged to estimate water PFOS and PFOA concentrations from the estimated K_d value and each observed soil concentration under the assumption of equilibrium conditions:

$$(\text{ng PFAA/L water}) = (\text{ng PFAA/kg soil})/\ K_d \quad (4)$$

For PFOS, the mean reported K_{oc} paired with the f_{oc} and PFOS data from 10 soil samples results in 10 estimates of equilibrium water PFOS concentration, with a mean 197 ng L^{-1} and a range of 58 to 472 ng L^{-1} (Figure 4). For PFOA, the mean reported K_{oc} paired with data from 8 soil

samples results in 8 estimates of equilibrium water PFOA concentration, with a mean of 1557 ng L^{-1} and a range of 120 to 5183 ng L^{-1} (Figure 4). For both PFOS and PFOA, the lowest values of these ranges are an order of magnitude higher than the 2019-2020 mean effluent concentrations (Figure *4*).

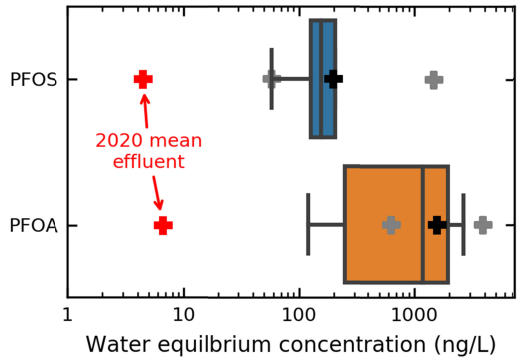

Figure 4. Box plots showing PFOS and PFOA water equilibrium concentrations calculated using Equations 2 and 4 with mean values of reported Koc and soil sample PFOS and PFOA concentrations and organic carbon content. Box edges represent the first and third quartiles, the line through each box represents the median, whiskers show the 10th and 90th percentiles, and the black crosses show the mean equilibrium concentration. The gray crosses show the concentrations calculated using the minimum and maximum reported Koc values, highlighting the variability introduced by the range in literature values. Red crosses show the mean effluent concentrations measured in 2020.

To illustrate the PFAA depth distributions that could develop under the three effluent concentration scenarios (1. observed in 2020 effluent, 2. lower bound from mass balance, and 3. averaged from an equilibrium assumption), predicted equilibrium profiles were calculated for PFOA and PFOS using the range of previously reported K_{oc} values and soil sample f_{oc}. With the 2020 effluent concentrations (PFOS 3.9 ng L^{-1}, PFOA 6.7 ng L^{-1}), predicted PFOS and PFOA equilibrium profiles are as much as one to two orders of magnitude lower than the observed profiles (Figure 5a and c). Using the lower bound for mass balance-derived effluent PFOS concentration (35 ng L^{-1}, PFOA 19 ng L^{-1}), the equilibrium profiles capture some of the observed

PFOS concentrations in soils above 0.5 m bgs, but fail to capture the deeper PFOS detections (Figure 5b). The mass balance-derived effluent PFOA concentration (19 ng L^{-1}) profile remains approximately an order of magnitude below the observed PFOA concentrations (Figure 5d). Profiles generated using the third scenario, the average equilibrium concentrations (PFOS 197 ng L^{-1}, PFOA 1557 ng L^{-1}, Figure 4), capture much of the observed PFOS profile (Figure 5b) as well as the deeper PFOA concentrations, while overpredicting the shallowest soil PFOA concentrations (Figure 5d).

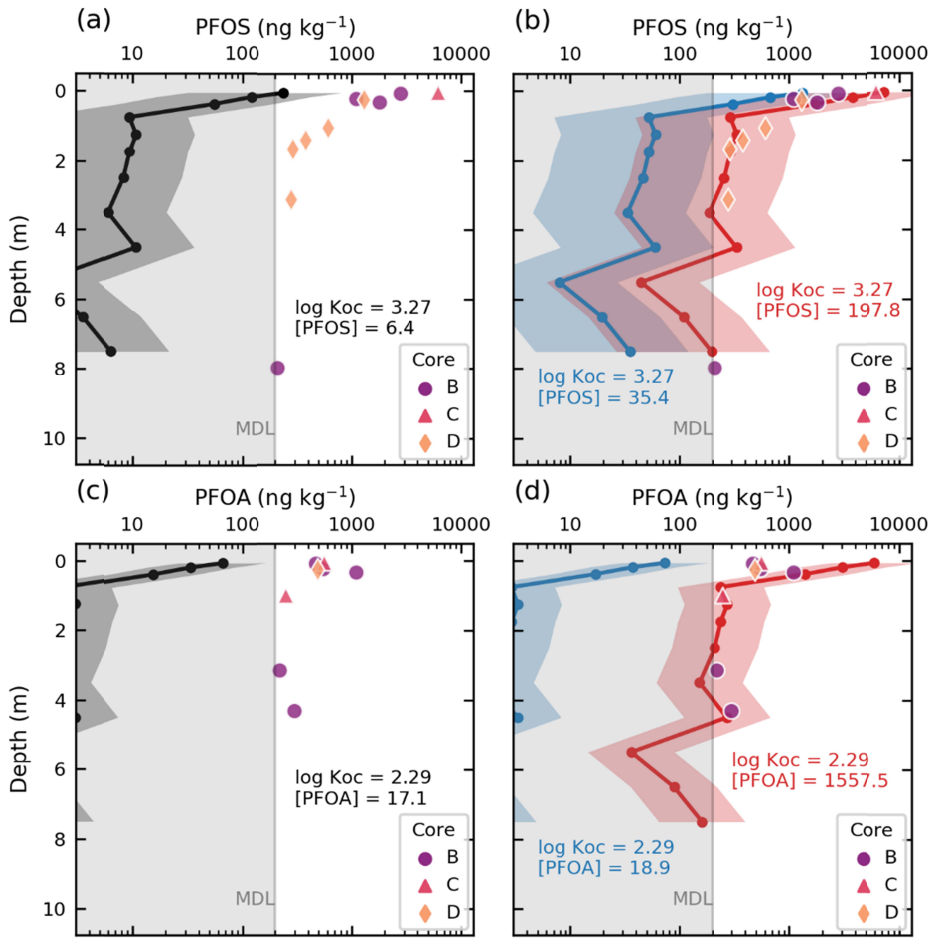

Figure 5. Observed PFOS and PFOA concentration profiles from the four Living Filter soil cores along with theoretical equilibrium profiles. Equilbrium profiles were generated pairing PFOS and PFOA effluent concentrations ([PFOS] and [PFOA]) with Kd profiles calculated from measured soil TOC profiles and reported Koc values (lines show the mean Koc and the filled

region is bounded by the minimum and maximum reported Koc values). The following effluent concentrations were used: (a) 2020 mean [PFOS] (black line and gray fill), (b) historical mass balance [PFOS] (blue line and fill) and soil-water equilibrium [PFOS] (from Figure 3-4) (red line and fill), (c) 2020 mean [PFOA] (black line and fill), (d) historical mass balance [PFOA] (blue line and fill) and soil-water equilibrium [PFOA] (from Figure 3-4) (red line and fill).

4.3 1-D transport models

For PFOS, cases with historical effluent concentrations between 60 and 180 ng L^{-1} (Figure S3) yielded the best fitting models (those with the lowest RMSE). These required the incorporation of PFOS K_{oc} near the upper bound of reported values ($10^{3.5}$ – $10^{3.8}$ L kg^{-1}). A subset of these low-RMSE PFOS transport models also predicted outflow at the base of the soil column consistent with the 2020 groundwater concentrations (Figure 6), with K_{oc} values of $10^{3.55}$ - $10^{3.7}$, and historical effluent concentrations between 70 and 170 ng L^{-1}.

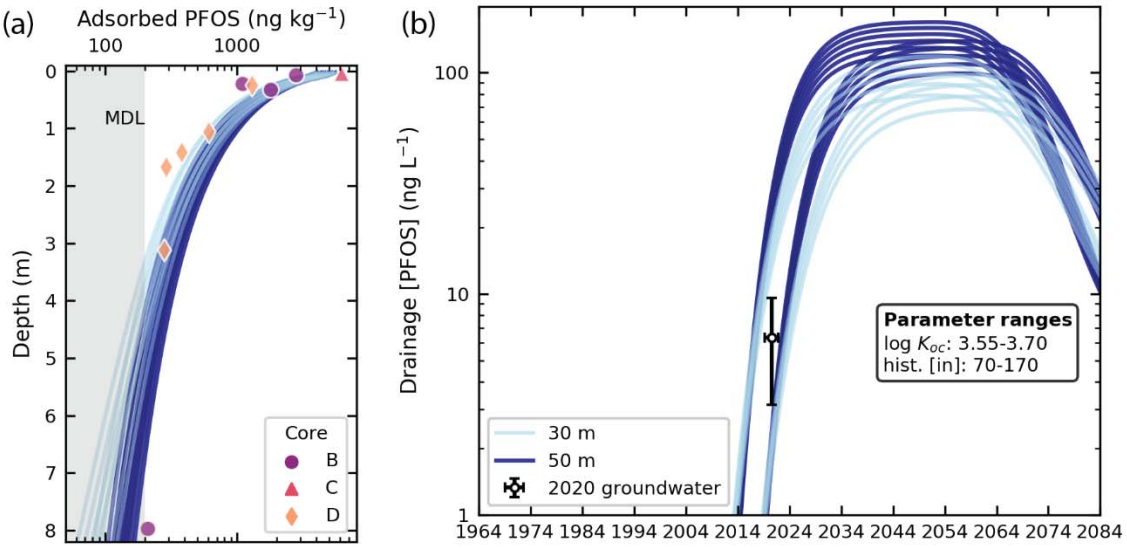

Figure 6. Modeling results for PFOS that capture both (a) the 2014 PFOS profile (RMSE < 1100 ng kg^{-1}) and (b) the 2020 groundwater PFOS concentration. Predicted concentrations of water draining at the base of the soil column are < 1 ng L^{-1} prior to ~2014.

Similarly, the models of PFOA transport with the lowest RMSEs required historical PFOA effluent concentrations between 600 and 2000 ng kg^{-1} (Figure S4) and were limited to those incorporating K_{oc} near the upper bound of values reported in the literature ($10^{2.4}$ – $10^{2.7}$ L kg^{-1}).

None of the models that best fit the 2014 soil PFOA profiles were also able to capture the 2020 groundwater concentrations (Figure 7).

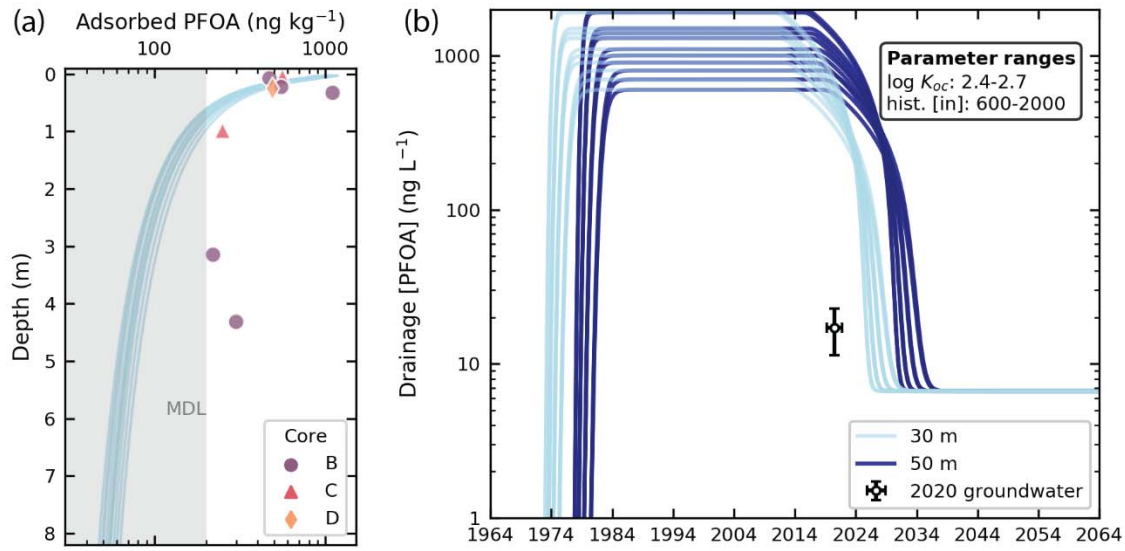

Figure 7. Modeling results for PFOA that capture both (a) the 2014 PFOA profile (RMSE < 370 ng kg^{-1}). None of these are able to adequately capture (b) the 2020 mean groundwater PFOA concentration.

To further explore modeling scenarios that could capture both the 2014 soil profile and 2020 groundwater observations without violating the reported range of K_{oc}, we adjusted the PFOA transport model. Specifically, we allowed applied water to percolate through the profile at a higher rate; through seven domain elements per week rather than one, but did not change the rate of surface application. This increased the modeled water flow velocity from ~8 cm per week to ~50 cm per week. The faster-flow model framework successfully captured PFOA profiles and groundwater concentrations while using log K_{oc} values of 2.4 and 2.5, and historical effluent concentrations of 1000 and 1300 ng L^{-1} (Figure 8). The increased downward flow rate could be accommodated by the Living Filter soils, for which mean saturated hydraulic conductivities are around 2 cm hour^{-1} (Andrews et al., 2016). The faster flow rate did not

drastically alter the outcome of modeled PFOS transport. The faster flow slightly improved the fit to the 2014 PFOS profile, while further constraining the original range of possible K_{oc} and historical concentrations: log K_{oc} was restricted to between 3.65 and 3.7, and the historical concentration to ~100 ng L^{-1} (Figure 9).

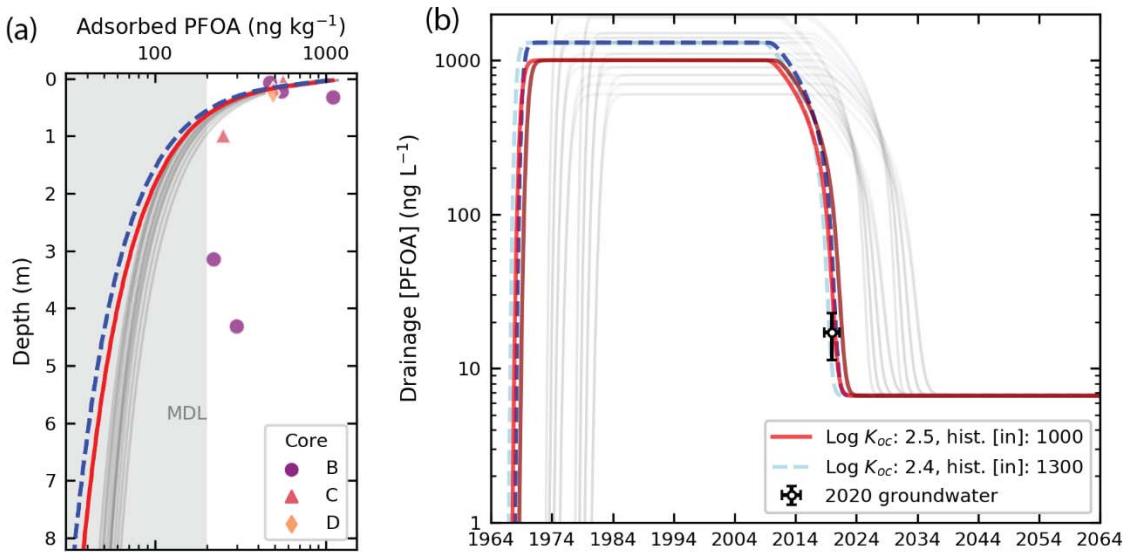

Figure 8. Two selected models incorporating a faster water flow rate (~50 cm per week rather than ~8 cm per week) to better capture both constraints on the transport history for PFOA: (a) the 2014 soil profile and (b) the 2020 groundwater concentrations. Shown are cases for depth to groundwater of 30 m (solid red line) and 50 m (solid dark red line), for Koc = $10^{2.5}$ and historical (pre-2000) concentration of 1000 ng L^{-1}. Also shown are the 30 m (dashed light blue line) and 50 m (dashed dark blue line) time series for Koc = $10^{2.4}$ and historical mean concentration of 1300 ng L^{-1}. Thin gray lines are the best fitting model results shown in Figure 7.

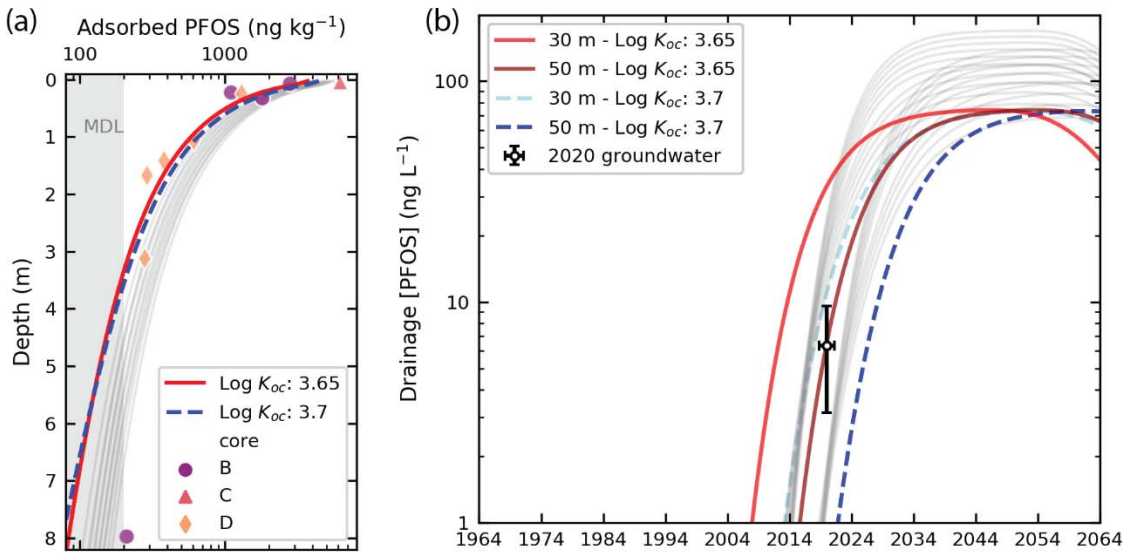

Figure 9. Results from the PFOS transport model incorporating the faster water flow rate (~50 cm per week rather than ~8 cm per week) that better captures transport history for PFOA. A log K_{oc} of 3.65-6.7 and historical (pre-2000) concentration of 75 ng L^{-1} best capture both (a) the 2014 soil profile and (b) the 2020 groundwater concentrations. Thin gray lines are the best fitting PFOS model results shown in Figure 6.

Despite the broadly successful model-data comparisons, one locality remained an outlier. None of the transport simulations were able to match the two PFOA detections in soil samples collected from core B at 3.1 and 4.3 m bgs. The laboratory-reported PFOA concentration for sample B-3.1 was on the edge of the laboratory MDL, so the reported value could overestimate the actual PFOA concentration. Further, the various simulations might not have matched B-4.3 concentration data because of the smoothed f_{oc} data used to define K_d in the model soil column. This did not capture the highest TOC values, including for B-4.3 (see Figure S1c). The modelled soil profile therefore underrepresents OC-based PFOA retention for high-TOC depth intervals in the core. This is evident from the computed PFOA equilibrium profiles (Figure *5*), which do incorporate the detailed depth variability in TOC that was lost in the smoothed fit used in our modeling, and which capture these higher PFOA concentrations.

5 Discussion

5.1 PFOS and PFOA adsorption

The K_{oc} values that generated the best fits for both the PFOS and PFOA profiles were consistent with those reported in the literature, but near the upper bound (Table S2). This is consistent with the previously noted trend that field-based studies tend to report higher PFAA K_{oc} values than laboratory studies (Weber et al., 2017; Zareitalabad et al., 2013). Past studies have ascribed this trend to additional sorption factors: 1) interaction with positively charged mineral surfaces, 2) interaction with air-water interfaces, and 3) sorption-desorption hysteresis.

The lack of correlations with soil texture, Al content, and Fe content in this study has been observed in other soils (Umeh et al., 2021), even though anion exchange capacity (AEC) does play a role in PFAA adsorption (Li et al., 2019; Umeh et al., 2021). While we did not measure soil AEC, the soil cores had relatively more kaolinite than other clays based on XRD analyses (Hagedorn, 2016). Kaolinite has the highest AEC potential of clays (Radcliffe & Šimůnek, 2010), so the Living Filter soils likely have some capacity to electrostatically retain negatively charged PFAAs. The six detected PFAAs have low pK_a values (Rayne & Forest, 2009), so their head groups will be negatively charged under the Living Filter soil pH range of 5 to 7 (Andrews et al., 2016) and able to interact with positively charged mineral surfaces. However, PFAAs can desorb more easily from mineral surfaces than from organics (Zhao et al., 2012), and PFAAs adsorbed to positively charged alumina plates could easily be removed by gentle rinsing with water. Given that a large amount of water infiltrates through the Living Filter each year (~260 cm yr^{-1} on average, more than double the average annual precipitation), any adsorption to clays or oxides is probably short-lived.

Laboratory column experiments have also shown that PFAA sorption at air-water interfaces (AWI) can greatly enhance PFAA retention in vadose zones (Lyu et al., 2018). While AWI sorption likely occurs at the Living Filter, the soils receive more water than a vadose zone under fully natural conditions (mean annual irrigation of ~160 cm yr^{-1} in addition to mean annual natural precipitation of ~100 cm yr^{-1}). During collection in December, the soil cores were near saturation, with a mean saturation ratio (soil volumetric water content over porosity) of 0.9. With the frequent irrigation and high soil water content at the Living Filter, it is likely that AWI in the soil profile is highly transient and PFAA retention at AWI is not a significant long-term retention factor.

The high K_{oc} values indicated by our modeling could also be field-based evidence for strong PFAA sorption-desorption hysteresis, which has been observed in soil and sediment batch experiments (Huiting Chen et al., 2016; Miao et al., 2017; Milinovic et al., 2015; Zhi & Liu, 2018). Lower desorption yields have been found for PFOS than PFOA, which was ascribed to the higher hydrophobicity of PFOS (Milinovic et al., 2015; Zhao et al., 2012). Notably, Huiting Chen et al. (2016) derived consistently higher PFAA K_{oc} values from desorption experiments, and they suggested sorption irreversibility can result from entrapment of PFAAs within organic matter solids, though the exact process is poorly understood. Sorption irreversibility could be responsible for consistently higher field-based PFAA K_{oc} values compared to lab-based, as speculated by Zareitalabad et al. (2013). Our field-based modeling results appear to support this notion, but there are too few published sorption-desorption data sets to confidently define hysteresis patterns and mechanisms, and the extent of hysteresis may be soil-specific. More work on PFAA sorption-desorption hysteresis is needed in both field and laboratory settings to

488 better define the importance of sorption hysteresis on PFAA retention under natural
489 conditions.

490 **5.2 Historical effluent PFOS and PFOA concentrations**

491 The reduction in global PFOS and PFOA production and use in commercial/industrial products
492 around 2000-2002 suggests that pre-2000 mean effluent concentrations at the Living Filter
493 should be higher than the observed current-day (2020) effluent concentrations. Our simple
494 mass balance analyses confirmed this, and yield required water equilibrium concentrations for
495 PFOS (197 ± 41 ng L^{-1}) and PFOA (1558 ± 608 ng L^{-1}) significantly higher than the mean 2020
496 effluent concentrations of 3.9 ng L^{-1} and 6.7 ng L^{-1}. Transport modeling informed by the 2014
497 soil profiles in tandem with groundwater data from 2020 further constrained pre-2000 PFOS
498 concentrations to 70 – 170 ng L^{-1} and pre-2000 PFOA concentrations to around 1000 – 1300 ng
499 L^{-1}.

500 Unfortunately, there are few pre-2000 records of wastewater effluent PFAA concentrations to
501 compare with our model results, especially for WWTPs that do not receive wastewater from
502 PFAA-related industry or manufacture. A 1999 study conducted by 3M measured PFOS and
503 PFOA in six WWTP effluents in the United States, four with known sources of PFAA exposure,
504 and two with no known PFAA sources (Sinclair & Kannan, 2006). One of the two control sites (in
505 Cleveland, TN) had PFOS and PFOA ranges of 417 – 454 ng L^{-1} and 665 – 674 ng L^{-1}, respectively,
506 and these values are similar to our estimated pre-2000 concentrations. More effluent records
507 are available from the mid-2000s, and while most reported effluent concentrations were below
508 our estimates, some non-industrial WWTPs have comparable PFOS and PFOA concentrations.
509 PFOS concentrations as high as 130 ng L^{-1} were observed in effluent from a Pacific Northwest

WWTP treating primarily domestic wastewater (Schultz, Barofsky, et al., 2006). PFOA concentrations as high as 1050 ng L^{-1} were measured in effluent from New York wastewater treatment plants that treated commercial and domestic wastewater in 2004 and 2005 (Sinclair & Kannan, 2006). Effluent from four California wastewater treatment plants had PFOS and PFOA concentrations that reached 187 ng L^{-1} and 185 ng L^{-1} in 2008 (Plumlee et al., 2008).

Clearly, pre-2000 effluents with PFOS and PFOA concentrations in the hundreds of ng L^{-1} have been discharged from WWTPs, with no known PFAA sources in their wastewater streams, and concentrations of similar magnitude have persisted after the PFOS and PFOA production phase-outs. Our pre-2000 effluent estimates lie in comparable ranges, so the Living Filter effluent concentrations estimated in this study align with reasonable loadings of PFAAs over the past three decades.

Rain-borne PFOS and PFOA are potential inputs to the Living Filter and were not accounted for in our models. If rainwater or airborne PFAAs are significant sources to the soil and vadose zone, our model estimates would represent overpredictions of past effluent concentrations. However, Scott et al., (2006) measured PFOA concentrations in precipitation across North American between 1998 and 1999, and found that rural areas rarely had PFOA concentrations above 5 ng L^{-1}. Given the rural landscape surrounding the Living Filter, rainfall PFAA contributions to the system were likely insignificant relative to effluent application. If 2020 precipitation concentrations were comparable to those measured in the late 1990s, precipitation could represent a PFAA source comparable to the effluent. However, even if 1990s precipitation concentrations were subtracted from all modeled effluent concentrations,

historical effluent concentrations would still need to be significantly higher than 2020 concentrations for the models to match the observed soil profiles.

5.3 Timing of PFOS and PFOA breakthrough and leaching

Because its high K_{oc}, PFOS movement through the soil profile in the best fitting models was significantly retarded, with breakthrough (defined by concentrations > 1 ng L^{-1} reaching the base of the soil column as groundwater recharge) only occurring around 2014 (Figure 6b). With the current effluent concentrations and rates of irrigation, future leaching of PFOS from the Living Filter is a distinct possibility. Our models predict that leaching, and concomitantly high PFOS concentrations in recharging groundwater at the base of the soil, will increase for the next ~20 years before reaching a maximum and ultimately beginning to decrease ~60 years after the ramp-down in effluent concentrations (Figure 6b).

The rate of leaching will depend on PFOS sorption irreversibility in these soils (lower leaching if high irreversibility), effluent irrigation rates (lower leaching if lower irrigation), and effluent PFOS concentrations (higher leaching if concentrations continue to decrease). While we cannot be certain of the exact timing and magnitudes of PFOS leaching from the Living Filter soils, our modeling effort suggests that the majority of PFOS mass applied over the history of the Living Filter remains stored in soils above the water table. This hypothesis can be tested by collecting additional soil cores and/or by continued monitoring of groundwater concentrations, and would be confirmed if soil PFOS concentrations are still relatively high and groundwater concentrations increase over the coming years. The long-term storage of PFOS in soils is an important consideration for other sites around the world that have received decadal-scale low

552 concentrations of PFOS from wastewater effluent. Even though effluent PFOS concentrations
553 are now low, legacy PFOS loads stored in soils may eventually affect groundwater quality.

554 In contrast, PFOA adsorption sites were saturated more rapidly, and thus more efficient
555 downward transport through the soil column. The best fitting models suggest that
556 breakthrough occurred well before the 2000s, perhaps even within a decade of the start of
557 irrigation (Figure 7b). This was largely because published K_{oc} values suggest organics do not
558 delay PFOA transport to the same degree as PFOS transport. If so, the 2020 groundwater PFOA
559 concentrations are likely not on the rising limb of the breakthrough curve. The observed 2020
560 groundwater concentrations more likely represent the declining limb of the PFOA time series as
561 a result of leaching (Figure 7b). A key implication is that the highest PFOA concentrations
562 leached to groundwater have likely already passed. Similar transport and leaching behavior
563 should be expected for other PFAAs with K_{oc} values comparable to or lower than PFOA, such as
564 PFHxA and PFPeA.

565 The transport model was built with two simplifying assumptions that could impact leaching
566 rates and timing. First, the model assumed water residence times are much longer than the
567 sorption rates of PFOS and PFOA, resulting in equilibrium sorption and aqueous concentrations
568 in pore waters. As discussed above, rapid adsorption has been observed in batch experiments
569 (Higgins & Luthy, 2006; Li et al., 2019). However, breakthrough curves from 1-D column flow
570 interruption experiments indicated rate-limited PFOS sorption under high flow rates (~0.4
571 m/day), but showed no evidence for nonequilibrium transport of PFOA (Guelfo et al., 2020). If
572 rate-limited PFOS and PFOA sorption behavior were present under the Living Filter soil
573 conditions, breakthrough could be affected by tailing and rebounding, resulting in longer

leaching timeframes and lower peak concentrations than those indicated by our modeling. Second, the transport model represents bulk transport processes and is parameterized with bulk physical and chemical properties collected from the soil cores. Therefore, the model does not capture potential leaching along preferential flow pathways, which would result in the model underestimating the timing and magnitudes of leached PFAA concentrations.

The storage and timing of transport illuminated by our analysis raises practical considerations and concerns for wastewater reuse by irrigation. While wastewater irrigation reduces effluent PFAA discharges to surface waters, depending on the production history and sorption behavior of individual PFAAs, wastewater irrigated soils may become long-term sources of PFAAs to groundwater. Even irrigated soils that currently appear to receive very low PFAA loads may have received much higher loads in the past.

Collection of soil samples from additional wastewater irrigation sites would allow for corroboration of this outcome and would help the scientific and policy communities assess and validate previously estimated PFAA environmental inventories. In addition to tracking legacy PFAAs like PFOS and PFOA, soils with different wastewater irrigation histories can provide information on the emission histories of newer compounds that replaced PFOS and PFOA, and are not currently regulated. Although TOC-exclusive sorption and piston flow models were satisfactory for testing PFAA transport behavior in this study, future work on these cores and other deep PFAA profiles would benefit from characterizing the impacts of preferential flow and other modes of PFAA soil sorption on transport, and incorporating those factors into more complex reactive transport models.

6 Conclusions

PFAA concentrations were measured in deep soil cores collected from a wastewater effluent spray field. Of the soil properties measured, soil total organic carbon content (TOC) is the best predictor of PFAA distributions in the soil profile, particularly for longer carbon chain PFAAs like PFOS and PFOA. Models of vertical flow, sorption and transport through the soil column yield best-fitting scenarios when K_{oc} is near the upper bound of values reported in the literature, and provide constraints on the time-averaged historical (pre-2000) effluent concentrations. The estimated concentrations are comparable to concentrations measured in some United States WWTP effluents in 1999 and the mid-2000s, indicating that concentrations in soils irrigated with wastewater can be used as records of historical PFAA loading. Even leaching fields that currently receive low PFAA loads may have received higher loads in the past. The model results also indicate stark differences in the leaching timing of PFAAs: the majority of PFOS mass applied over the history of the Living Filter likely remains stored in soils above the water table, while the bulk of the PFOA mass has likely already leached to groundwater. Depending on the production history and sorption behavior of individual PFAAs, wastewater irrigated soils can become a long-term source of PFAAs to groundwater.

7 Acknowledgements

This project was supported by a grant from The Pennsylvania State University Office of the Physical Plant to KJ, DS, and KF. We would like to thank Jake Hagedorn for his collection and original analysis of the cores, which was supported by a grant from The Pennsylvania State University's Sustainability Institute. We thank David Swisher for his input on Living Filter operations. We also thank Roman DiBiase for his insightful review of an early version of the manuscript.

8 Open Research

The data and Python code used for modeling PFAA transport in the study can be found on Zenodo (Jahn, 2022). Python packages used include Matplotlib (Hunter, 2007), NumPy (Harris et al., 2020), Pandas (McKinney, 2010; Reback et al., 2020), Seaborn (Waskom, 2021), and SciPy (Virtanen et al., 2020).

9 References

Anderson, R. H., Adamson, D. T., & Stroo, H. F. (2019). Partitioning of poly- and perfluoroalkyl substances from soil to groundwater within aqueous film-forming foam source zones. *Journal of Contaminant Hydrology*, *220*, 59–65. https://doi.org/10.1016/j.jconhyd.2018.11.011

Andrews, D. M., Robb, T., Elliott, H., & Watson, J. E. (2016). Impact of long-term wastewater irrigation on the physicochemical properties of humid region soils: “The Living Filter” site case study. *Agricultural Water Management*, *178*, 239–247. https://doi.org/10.1016/j.agwat.2016.10.001

Ayers, B., Elkin, K., Kibuye, F., & Gall, H. E. (2017). Pharmaceuticals at Penn State’s Living Filter: From Wastewater to Groundwater. In *2017 Spokane, Washington July 16 - July 19, 2017*. American Society of Agricultural and Biological Engineers. https://doi.org/10.13031/aim.201700255

Bekele, D. N., Liu, Y., Donaghey, M., Umeh, A., Arachchige, C. S. V., Chadalavada, S., & Naidu, R. (2020). Separation and Lithological Mapping of PFAS Mixtures in the Vadose Zone at a Contaminated Site. *Frontiers in Water*, *2*, 597810. https://doi.org/10.3389/frwa.2020.597810

Brusseau, M. L., Yan, N., Van Glubt, S., Wang, Y., Chen, W., Lyu, Y., et al. (2019). Comprehensive retention model for PFAS transport in subsurface systems. *Water Research*, *148*, 41–50. https://doi.org/10.1016/j.watres.2018.10.035

Brusseau, M. L., Anderson, R. H., & Guo, B. (2020). PFAS concentrations in soils: Background levels versus contaminated sites. *Science of The Total Environment*, *740*, 140017. https://doi.org/10.1016/j.scitotenv.2020.140017

Butts, C., & Moore, E. S. (1936). *Geology and mineral resources of the Bellefonte quadrangle, Pennsylvania* (Geological Survey Bulletin No. 855). U.S. Geological Survey. https://doi.org/10.3133/b855

Chen, Hongrui, Peng, H., Yang, M., Hu, J., & Zhang, Y. (2017). Detection, Occurrence, and Fate of Fluorotelomer Alcohols in Municipal Wastewater Treatment Plants. *Environmental Science & Technology*, *51*(16), 8953–8961. https://doi.org/10.1021/acs.est.7b00315

Chen, Huiting, Reinhard, M., Nguyen, V. T., & Gin, K. Y.-H. (2016). Reversible and irreversible sorption of perfluorinated compounds (PFCs) by sediments of an urban reservoir. *Chemosphere*, *144*, 1747–1753. https://doi.org/10.1016/j.chemosphere.2015.10.055

Chirikona, F., Filipovic, M., Ooko, S., & Orata, F. (2015). Perfluoroalkyl acids in selected wastewater treatment plants and their discharge load within the Lake Victoria basin in Kenya. *Environmental Monitoring and Assessment*, *187*(5), 238. https://doi.org/10.1007/s10661-015-4425-6

Dauchy, X., Boiteux, V., Colin, A., Hémard, J., Bach, C., Rosin, C., & Munoz, J.-F. (2019). Deep seepage of per- and polyfluoroalkyl substances through the soil of a firefighter training

site and subsequent groundwater contamination. *Chemosphere*, *214*, 729–737. https://doi.org/10.1016/j.chemosphere.2018.10.003

Dieter, C. A., Maupin, M. A., Caldwell, R. R., Harris, M. A., Ivahnenko, T. I., Lovelace, J. K., et al. (2018). *Estimated use of water in the United States in 2015* (Circular No. 1441) (p. 65). Reston, VA: U.S. Geological Survey. Retrieved from https://doi.org/10.3133/cir1441

Gallen, C., Eaglesham, G., Drage, D., Nguyen, T. H., & Mueller, J. F. (2018). A mass estimate of perfluoroalkyl substance (PFAS) release from Australian wastewater treatment plants. *Chemosphere*, *208*, 975–983. https://doi.org/10.1016/j.chemosphere.2018.06.024

Guelfo, J. L., Wunsch, A., McCray, J., Stults, J. F., & Higgins, C. P. (2020). Subsurface transport potential of perfluoroalkyl acids (PFAAs): Column experiments and modeling. *Journal of Contaminant Hydrology*, *233*, 103661. https://doi.org/10.1016/j.jconhyd.2020.103661

Guo, B., Zeng, J., & Brusseau, M. L. (2020). A Mathematical Model for the Release, Transport, and Retention of Per- and Polyfluoroalkyl Substances (PFAS) in the Vadose Zone. *Water Resources Research*, 2019WR026667. https://doi.org/10.1029/2019WR026667

Hagedorn, J. G. (2016, August). *The Living Filter: monitoring nitrate accumulation after 50 years of waster irrigation* (Master of Science). The Pennsylvania State University.

Harris, C. R., Millman, K. J., van der Walt, S. J., Gommers, R., Virtanen, P., Cournapeau, D., et al. (2020). Array programming with NumPy. *Nature*, *585*(7825), 357–362. https://doi.org/10.1038/s41586-020-2649-2

Hellsing, M. S., Josefsson, S., Hughes, A. V., & Ahrens, L. (2016). Sorption of perfluoroalkyl substances to two types of minerals. *Chemosphere*, *159*, 385–391. https://doi.org/10.1016/j.chemosphere.2016.06.016

683 Higgins, C. P., & Luthy, R. G. (2006). Sorption of Perfluorinated Surfactants on Sediments.
684 *Environmental Science & Technology*, *40*(23), 7251–7256.
685 https://doi.org/10.1021/es061000n
686 Houtz, E. F., Sutton, R., Park, J.-S., & Sedlak, M. (2016). Poly- and perfluoroalkyl substances in
687 wastewater: Significance of unknown precursors, manufacturing shifts, and likely AFFF
688 impacts. *Water Research*, *95*, 142–149. https://doi.org/10.1016/j.watres.2016.02.055
689 Hunter, J. D. (2007). Matplotlib: A 2D Graphics Environment. *Computing in Science &*
690 *Engineering*, *9*(3), 90–95. https://doi.org/10.1109/MCSE.2007.55
691 Jahn, K. (2022). Storage, transport, and fate of perfluoroalkyl acids (PFAAs) in a wastewater re-
692 use and groundwater recharge system - data and code. Zenodo [Dataset and Software].
693 https://doi.org/10.5281/zenodo.7439554
694 Lattman, L. H., & Parizek, R. R. (1964). Relationship between fracture traces and the occurrence
695 of ground water in carbonate rocks. *Journal of Hydrology*, *2*(2), 73–91.
696 https://doi.org/10.1016/0022-1694(64)90019-8
697 Li, F., Fang, X., Zhou, Z., Liao, X., Zou, J., Yuan, B., & Sun, W. (2019). Adsorption of perfluorinated
698 acids onto soils: Kinetics, isotherms, and influences of soil properties. *Science of The*
699 *Total Environment*, *649*, 504–514. https://doi.org/10.1016/j.scitotenv.2018.08.209
700 Loganathan, B. G., Sajwan, K. S., Sinclair, E., Senthil Kumar, K., & Kannan, K. (2007).
701 Perfluoroalkyl sulfonates and perfluorocarboxylates in two wastewater treatment
702 facilities in Kentucky and Georgia. *Water Research*, *41*(20), 4611–4620.
703 https://doi.org/10.1016/j.watres.2007.06.045

Lyu, Y., Brusseau, M. L., Chen, W., Yan, N., Fu, X., & Lin, X. (2018). Adsorption of PFOA at the Air–Water Interface during Transport in Unsaturated Porous Media. *Environmental Science & Technology*, *52*(14), 7745–7753. https://doi.org/10.1021/acs.est.8b02348

McKinney, W. (2010). Data Structures for Statistical Computing in Python. In *Proceedings of the 9th Python in Science Conference* (pp. 56–61). Austin, Texas. https://doi.org/10.25080/Majora-92bf1922-00a

Miao, Y., Guo, X., Dan Peng, Fan, T., & Yang, C. (2017). Rates and equilibria of perfluorooctanoate (PFOA) sorption on soils from different regions of China. *Ecotoxicology and Environmental Safety*, *139*, 102–108. https://doi.org/10.1016/j.ecoenv.2017.01.022

Milinovic, J., Lacorte, S., Vidal, M., & Rigol, A. (2015). Sorption behaviour of perfluoroalkyl substances in soils. *Science of The Total Environment*, *511*, 63–71. https://doi.org/10.1016/j.scitotenv.2014.12.017

Mroczko, O., Preisendanz, H. E., Wilson, C., Mashtare, M. L., Elliott, H. A., Veith, T. L., et al. (2022). Spatiotemporal patterns of PFAS in water and crop tissue at a beneficial wastewater reuse site in central Pennsylvania. *Journal of Environmental Quality*, *51*(6), 1282–1297. https://doi.org/10.1002/jeq2.20408

Parizek, R. R., Kardos, L. T., Sopper, W. E., Myers, E. A., Davis, D. E., Farrell, M. A., & Nesbitt, J. B. (1967). *Waste water renovation and conservation* (The Pennsylvania State University Studies No. 23). University Park, Pennsylvania: The Pennsylvania State University.

724 Paul, A. G., Jones, K. C., & Sweetman, A. J. (2009). A First Global Production, Emission, And
725 Environmental Inventory For Perfluorooctane Sulfonate. *Environmental Science &*
726 *Technology*, *43*(2), 386–392. https://doi.org/10.1021/es802216n
727 Plumlee, M. H., Larabee, J., & Reinhard, M. (2008). Perfluorochemicals in water reuse.
728 *Chemosphere*, *72*(10), 1541–1547. https://doi.org/10.1016/j.chemosphere.2008.04.057
729 Prevedouros, K., Cousins, I. T., Buck, R. C., & Korzeniowski, S. H. (2006). Sources, Fate and
730 Transport of Perfluorocarboxylates. *Environmental Science & Technology*, *40*(1), 32–44.
731 https://doi.org/10.1021/es0512475
732 Radcliffe, D. E., & Šimůnek, J. (2010). *Soil Physics with HYDRUS* (First). Boca Raton, Florida: CRC
733 Press - Taylor & Francis Group.
734 Rayne, S., & Forest, K. (2009). Theoretical studies on the pK~a~ values of perfluoroalkyl
735 carboxylic acids: Chain helicity. *Nature Precedings*.
736 https://doi.org/10.1038/npre.2009.3829.1
737 Reback, J., McKinney, W., jbrockmendel, Bossche, J. V. den, Augspurger, T., Cloud, P., et al.
738 (2020, February 5). pandas-dev/pandas: Pandas 1.0.1. Zenodo.
739 https://doi.org/10.5281/zenodo.3644238
740 Schultz, M. M., Higgins, C. P., Huset, C. A., Luthy, R. G., Barofsky, D. F., & Field, J. A. (2006).
741 Fluorochemical Mass Flows in a Municipal Wastewater Treatment Facility.
742 *Environmental Science & Technology*, *40*(23), 7350–7357.
743 https://doi.org/10.1021/es061025m
744 Schultz, M. M., Barofsky, D. F., & Field, J. A. (2006). Quantitative Determination of Fluorinated
745 Alkyl Substances by Large-Volume-Injection Liquid Chromatography Tandem Mass

Spectrometry - Characterization of Municipal Wastewaters. *Environmental Science & Technology*, *40*(1), 289–295. https://doi.org/10.1021/es051381p

Scott, B. F., Spencer, C., Mabury, S. A., & Muir, D. C. G. (2006). Poly and Perfluorinated Carboxylates in North American Precipitation †. *Environmental Science & Technology*, *40*(23), 7167–7174. https://doi.org/10.1021/es061403n

Siddiqui, S. H., & Parizek, R. R. (1971). Hydrogeologic Factors Influencing Well Yields in Folded and Faulted Carbonate Rocks in Central Pennsylvania. *Water Resources Research*, *7*(5), 1295–1312. https://doi.org/10.1029/WR007i005p01295

Sinclair, E., & Kannan, K. (2006). Mass Loading and Fate of Perfluoroalkyl Surfactants in Wastewater Treatment Plants. *Environmental Science & Technology*, *40*(5), 1408–1414. https://doi.org/10.1021/es051798v

Smith, R. E. (1969). Petrography-Porosity Relations in Carbonate-Quartz System, Gatesburg Formation (Late Cambrian), Pennsylvania. *AAPG Bulletin*, *53*. https://doi.org/10.1306/5D25C609-16C1-11D7-8645000102C1865D

Sunderland, E. M., Hu, X. C., Dassuncao, C., Tokranov, A. K., Wagner, C. C., & Allen, J. G. (2019). A review of the pathways of human exposure to poly- and perfluoroalkyl substances (PFASs) and present understanding of health effects. *Journal of Exposure Science & Environmental Epidemiology*, *29*(2), 131–147. https://doi.org/10.1038/s41370-018-0094-1

Umeh, A. C., Naidu, R., Shilpi, S., Boateng, E. B., Rahman, A., Cousins, I. T., et al. (2021). Sorption of PFOS in 114 Well-Characterized Tropical and Temperate Soils: Application of

767 Multivariate and Artificial Neural Network Analyses. *Environmental Science &*
768 *Technology*, *55*(3), 1779–1789. https://doi.org/10.1021/acs.est.0c07202
769 Virtanen, P., Gommers, R., Oliphant, T. E., Haberland, M., Reddy, T., Cournapeau, D., et al.
770 (2020). SciPy 1.0: fundamental algorithms for scientific computing in Python. *Nature*
771 *Methods*, *17*(3), 261–272. https://doi.org/10.1038/s41592-019-0686-2
772 Walker, C., & Lin, H. S. (2008). Soil property changes after four decades of wastewater
773 irrigation: A landscape perspective. *CATENA*, *73*(1), 63–74.
774 https://doi.org/10.1016/j.catena.2007.09.002
775 Waskom, M. L. (2021). seaborn: statistical data visualization. *Journal of Open Source Software*,
776 *6*(60), 3021. https://doi.org/10.21105/joss.03021
777 Weber, A. K., Barber, L. B., LeBlanc, D. R., Sunderland, E. M., & Vecitis, C. D. (2017).
778 Geochemical and Hydrologic Factors Controlling Subsurface Transport of Poly- and
779 Perfluoroalkyl Substances, Cape Cod, Massachusetts. *Environmental Science &*
780 *Technology*, *51*(8), 4269–4279. https://doi.org/10.1021/acs.est.6b05573
781 Wood, C. R. (1980). *Summary groundwater resources of Centre County, Pennsylvania*
782 (Pennsylvania Geological Survey Water Resource Report No. 48) (p. 69). Harrisburg:
783 Pennsylvania Geological Survey.
784 Zareitalabad, P., Siemens, J., Hamer, M., & Amelung, W. (2013). Perfluorooctanoic acid (PFOA)
785 and perfluorooctanesulfonic acid (PFOS) in surface waters, sediments, soils and
786 wastewater – A review on concentrations and distribution coefficients. *Chemosphere*,
787 *91*(6), 725–732. https://doi.org/10.1016/j.chemosphere.2013.02.024

Zhang, W., Zhang, Y., Taniyasu, S., Yeung, L. W. Y., Lam, P. K. S., Wang, J., et al. (2013). Distribution and fate of perfluoroalkyl substances in municipal wastewater treatment plants in economically developed areas of China. *Environmental Pollution*, *176*, 10–17. https://doi.org/10.1016/j.envpol.2012.12.019

Zhang, X., Zhang, Y., Dassuncao, C., Lohmann, R., & Sunderland, E. M. (2017). North Atlantic Deep Water formation inhibits high Arctic contamination by continental perfluorooctane sulfonate discharges: North Atlantic PFOS Inputs to the Arctic. *Global Biogeochemical Cycles*, *31*(8), 1332–1343. https://doi.org/10.1002/2017GB005624

Zhao, L., Zhu, L., Yang, L., Liu, Z., & Zhang, Y. (2012). Distribution and desorption of perfluorinated compounds in fractionated sediments. *Chemosphere*, *88*(11), 1390–1397. https://doi.org/10.1016/j.chemosphere.2012.05.062

Zhi, Y., & Liu, J. (2018). Sorption and desorption of anionic, cationic and zwitterionic polyfluoroalkyl substances by soil organic matter and pyrogenic carbonaceous materials. *Chemical Engineering Journal*, *346*, 682–691. https://doi.org/10.1016/j.cej.2018.04.042

Zimmermann, C. F., Keefe, C. W., & Bashe, J. (1997, September). Method 440.0 Determination of Carbon and Nitrogen in Sediments and Particulates of Estuarine/Coastal Waters Using Elemental Analysis, Revision 1.4. U.S. Environmental Protection Agency. Retrieved from https://cfpub.epa.gov/si/si_public_record_report.cfm?Lab=NERL&dirEntryId=309418